PTEP

Prog. Theor. Exp. Phys. **2019**, 053G01 (11 pages)
DOI: 10.1093/ptep/ptz024

# Formation of hollow ion beams of various shapes using multipole magnets

Yosuke Yuri[1,*], Mitsuhiro Fukuda[2], and Takahiro Yuyama[1]

[1]*Takasaki Advanced Radiation Research Institute, National Institutes for Quantum and Radiological Science and Technology, 1233 Watanuki-machi, Takasaki 370-1292, Japan*
[2]*Research Center for Nuclear Physics, Osaka University, 10-1 Mihogaoka, Ibaraki 567-0047, Japan*
[*]E-mail: yuri.yosuke@qst.go.jp

Received February 1, 2019; Revised March 4, 2019; Accepted March 11, 2019; Published May 11, 2019

This study describes a novel and simple beam-focusing method for the formation of a charged-particle beam with a hollow transverse intensity distribution using the nonlinear focusing force of multipole magnets in a beam transport line. The dynamic behavior of the beam focused by multipole magnets is theoretically investigated to predict the phase-space shape and spatial profile of the hollow beam. It is shown numerically and experimentally that the hollow beam has a steep peak at the peripheral edge and high contrast between the edge peak intensity and the intensity near the beam center. Depending on the order and strength of the applied nonlinear multipole field, the cross-sectional shape of the hollow beam can be diversely transformed, e.g., into an ellipse, a rounded rectangle, a rhombus for octupole focusing, or a triangle for sextupole focusing. The present beam-formation method, applicable to various charged-particle beams of different parameters such as the particle species, kinetic energy, and time structure, enables the shaping of the transverse profile that can never be realized through conventional linear beam optics.

Subject Index G02, G10, G12

## 1. Introduction

The transverse spatial intensity distribution of a charged-particle beam generated by a particle accelerator is an essential experimental parameter that should be freely controlled based on the purpose of utilization. In fact, to meet user demands, the intensity distribution of an energetic ion beam extracted, e.g., from cyclotrons and synchrotrons is tailored into various shapes and distributions using different types of magnets and/or other apparatuses such as collimators and scatterers. Examples include precise focusing on a small spot ($< 1\mu$m) for targeted irradiation of biological cells [1,2] and uniformly expanding to a large area (a few tens of cm) for cancer therapy [3,4]. A *hollow beam* is another example of such a tailored beam that is sometimes required for advanced applications. In general, the hollow beam can be defined as a beam with a higher intensity in the peripheral (radially outer) part than that in the central (inner) part of a transverse beam cross-section, which is qualitatively different from spot beam wobbling [5] in that the beam itself has a hollow intensity distribution. Such extraordinary beams were experimentally generated in the study of high-energy-density physics and heavy-ion inertial fusion through the strong nonlinear focusing of a plasma lens [6,7]. A hollow circular profile of 1–2 cm in diameter was formed by matching the short pulse of a high-energy heavy-ion beam to the timing of the plasma lens discharge. For low beam energy, an electron gun dedicated to producing pulsed hollow electron beams was developed for the halo collimation of high-energy intense beams [8]. In addition, a hollow-beam profile was observed in the

transport process of high-current heavy-ion beams extracted from electron cyclotron resonance ion sources [9,10]. This phenomenon is attributed to the strong space-charge effect due to the coexistence of ion beams with different mass-to-charge ratios. The effect of the aberration of an einzel lens was also reported [11]. Although a few methods of generating hollow beams have been studied, their applicability and controllability are rather limited. For example, there has been no practical method that can be applied to a continuous beam from a cyclotron.

Here, multipole magnets that produce a nonlinear focusing force are employed as a novel method to form hollow beams. Most previous works on beam-profile manipulation using multipole (mainly octupole) magnets aimed to form a beam with large-area uniform transverse intensity distributions [12–15]. No comprehensive discussions have previously been made on the formation of hollow beams using multipole magnets and their parameter dependences, although the hollowing of the profile has been recognized during uniform-beam formation. In this paper, we demonstrate the formation of hollow beams with different cross-sectional shapes and steep edge peaks based on the order and strengths of the applied multipole magnets. In contrast to the existing methods mentioned above, the present method is simple and thus has higher applicability and controllability because the source of the nonlinear force is the magnetostatic field produced by multipole magnets.

The paper is organized as follows: In Sect. 2, we first derive analytical expressions to predict the dynamic behavior of a beam focused with multipole magnets. Then, in Sect. 3, the results of particle tracking simulations are described to verify the theoretical prediction. In Sect. 4, various hollow beams are demonstrated experimentally. Section 5 is devoted to a discussion on the parameter dependence of the hollow-beam characteristics. Finally, the present results are summarized in Sect. 6.

## 2. Theoretical consideration

The behavior of a beam focused with multipole magnets in a beam transport line is analytically investigated. We take a step from Ref. [16] toward deriving approximate expressions on the phase-space shape and spatial profile of the multipole-focused beam. For brevity, the 1D motion of an on-axis particle is considered here, although the betatron motion between the horizontal and vertical directions is actually coupled by multipole magnets. As will be shown later, the 1D treatment is sufficient for the present purpose to understand the primary dynamics of the multipole-focused beam.

Consider that the beam travels through the transport line including two thin octupole magnets located separately before a target. The on-target position $x_t$ and momentum $p_t$ of a particle focused by the two octupole magnets can be determined using the following matrix multiplication:

$$\begin{pmatrix} x_{\mathrm{t}} \\ p_{\mathrm{t}} \end{pmatrix} = \mathbf{T} \begin{pmatrix} x_2 \\ p_2 - K_{\mathrm{O2}} x_2^3/6 \end{pmatrix}, \begin{pmatrix} x_2 \\ p_2 \end{pmatrix} = \mathbf{M} \begin{pmatrix} x_1 \\ p_1 - K_{\mathrm{O1}} x_1^3/6 \end{pmatrix}, \tag{1}$$

where $(x_1, p_1)$ and $(x_2, p_2)$ are the particle's coordinates at the first and second octupole magnets, respectively. **M** and **T** are the transfer matrices of the linear optics from the first octupole magnet to the second, and from the second to the target, respectively. $K_{\mathrm{O1(O2)}}$ is the integrated strength of the first (second) octupole magnet. Assuming $p_1 = -(\alpha_1/\beta_1)\, x_1$, which is a reasonable approximation when $|\alpha_1| \gg 0$ at the first octupole magnet, we obtain the on-target coordinate $(x_t, p_t)$ of the particle

as follows:

$$x_{\rm t} = \sqrt{\frac{\beta_{\rm t}}{\beta_1}}\cos(\varphi+\theta)\,x_1 - \frac{K_{\rm O1}}{6}\sqrt{\beta_1\beta_{\rm t}}\sin(\varphi+\theta)\,x_1^3 - \frac{K_{\rm O2}}{6}\sqrt{\beta_2\beta_{\rm t}}\sin\theta\left(\sqrt{\frac{\beta_2}{\beta_1}}\cos\varphi x_1 - \frac{K_{\rm O1}}{6}\sqrt{\beta_1\beta_2}\sin\varphi x_1^3\right)^3, \tag{2}$$

$$p_{\rm t} = -\frac{1}{\sqrt{\beta_1\beta_{\rm t}}}\{\sin(\varphi+\theta)+\alpha_{\rm t}\cos(\varphi+\theta)\}\,x_1 - \frac{K_{\rm O1}}{6}\sqrt{\frac{\beta_1}{\beta_{\rm t}}}\{\cos(\varphi+\theta)-\alpha_{\rm t}\sin(\varphi+\theta)\}\,x_1^3 - \frac{K_{\rm O2}}{6}\sqrt{\frac{\beta_2}{\beta_{\rm t}}}(\cos\theta-\alpha_{\rm t}\sin\theta)\left(\sqrt{\frac{\beta_2}{\beta_1}}\cos\varphi x_1 - \frac{K_{\rm O1}}{6}\sqrt{\beta_1\beta_2}\sin\varphi x_1^3\right)^3, \tag{3}$$

where $\alpha$ and $\beta$ are the Twiss parameters in the linear beam optics. $\varphi$ and $\theta$ are the linear-optics phase advances from the first octupole magnet to the second and from the second one to the target, respectively. The suffixes 1, 2, and t of the Twiss parameters denote the location along the beam line, i.e., the first octupole magnet, second octupole magnet, and target, respectively. The transfer matrices **M** and **T** have been rewritten using the Twiss parameters and phase advances. From Eqs. (2) and (3), the phase-space shape (not distribution) of the octupole-focused beam on the target can be determined numerically with respect to an arbitrary $x_1$. In other words, these equations approximately predict how the major axis of the original beam's phase-space ellipse develops after the octupole focusing.

Moreover, the on-target real-space intensity distribution $\rho_{\rm t}$ of the octupole-focused beam can be related to the initial distribution $\rho_1$ at the first octupole magnet as follows [16]:

$$\rho_{\rm t} = \rho_1\left(\frac{dx_{\rm t}}{dx_1}\right)^{-1}. \tag{4}$$

For example, $\rho_1$ can be a Gaussian distribution $\rho_1 = 1/\sqrt{2\pi\varepsilon\beta_1}\times{\rm Exp}\left[-x_1^2/(2\varepsilon\beta_1)\right]$, where $\varepsilon$ is the un-normalized root-mean-square (rms) emittance.

## 3. Tracking simulation

### *3.1. Simulation conditions*

Numerical tracking simulations were performed, paying particular attention to the particle motion in the transverse direction, to reveal various characteristics of the hollow beam and confirm the theoretical expectations above. In the simulation, a particle-tracking code that can consider the nonlinear magnetic fields produced by multipole magnets (up to dodecapole) was employed [16]. We adopted the lattice structure of the high-energy beam transport line in the azimuthally varying field cyclotron ($K$-number of 110 MeV) facility [17] of the Takasaki Ion Accelerators for Advanced Radiation Application (TIARA), National Institutes for Quantum and Radiological Science and Technology, where the hollow-beam formation experiment was performed. Two octupole and two sextupole magnets were installed together with some quadrupole magnets near the end of the beam line, whose path length was about 43 m. The detailed parameters of the beam line and multipole magnets are summarized in Ref. [14]. Figure 1 shows a typical design of the linear beam envelope

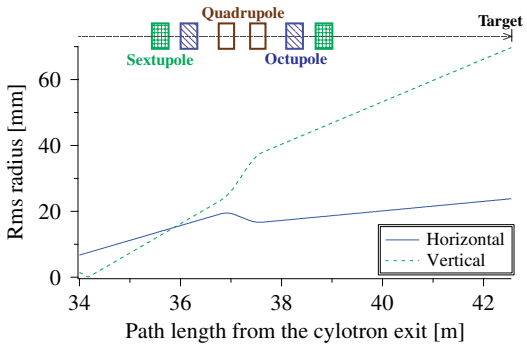


**Fig. 1.** Schematic layout of magnets and transverse beam envelope calculation near the hollow-beam formation target. The assumed rms emittance is $2\pi$ mm·mrad in the horizontal direction and $1\pi$ mm·mrad in the vertical direction, according to past measurements. Two sets of sextupole and octupole magnets have been installed beside the final quadrupole doublet. The maximum field gradients of the sextupole and octupole magnets are $3.1 \times 10^2$ T/m$^2$ and $1.3 \times 10^4$ T/m$^3$, respectively, and their effective axial length is 0.33 m.

**Table 1.** Beam and transport line parameters in the tracking simulation.

| | Horizontal | Vertical |
|---|---|---|
| Rms emittance $\varepsilon$ (un-normalized) | $2\pi$ mm·mrad | $1\pi$ mm·mrad |
| Average beta function $\beta_1$ at the 1st octupole magnet | 130 m | 350 m |
| Average beta function $\beta_2$ at the 2nd octupole magnet | 150 m | 1900 m |
| Beta function $\beta_t$ at the target | 277 m | 5360 m |
| Alpha function $\alpha_t$ at the target | −16.9 | −496 |
| Phase advance $\varphi$ from the 1st octupole magnet to the 2nd one | 0.013 rad | 0.0025 rad |
| Phase advance $\theta$ from the 2nd octupole magnet to the target | 0.021 rad | 0.0013 rad |

near the target. The main parameters of the beam and beam line in the simulation are summarized in Table 1. The major difference between the beam optics for hollow-beam and uniform-beam formations is the existence of the betatron oscillation's horizontal–vertical coupling at the multipole magnets in the former. The betatron coupling is crucial for the formation of a hollow beam with various cross-sectional shapes, as will be shown later.

As for the initial conditions of the beam (10 MeV proton), the transverse intensity distribution was assumed to be Gaussian, and the un-normalized rms emittance $\varepsilon$ was set as $2\pi$ mm·mrad in the horizontal direction and $1\pi$ mm·mrad in the vertical direction, according to past measurements [14]. The longitudinal momentum spread of the beam was ignored unless otherwise noted. The number of particles tracked in the simulation was $10^7$ to obtain the intensity distribution with a sufficiently high precision.

### *3.2. Results*

Figure 2 presents the on-target profiles of the beam focused by one or two octupole magnets. When one octupole magnet is turned on (with the other quadrupole magnets), the tail of the original beam profile is folded toward the inside on (and near) the horizontal and vertical axes owing to the focusing effect based on the polarity of the octupole magnetic field, as shown in Fig. 2(a). A steep peak has already been generated at the edge of the beam. In the oblique directions, on the other hand, particles are defocused, and the four "tips" at which the particle density is locally high are generated owing to betatron coupling.

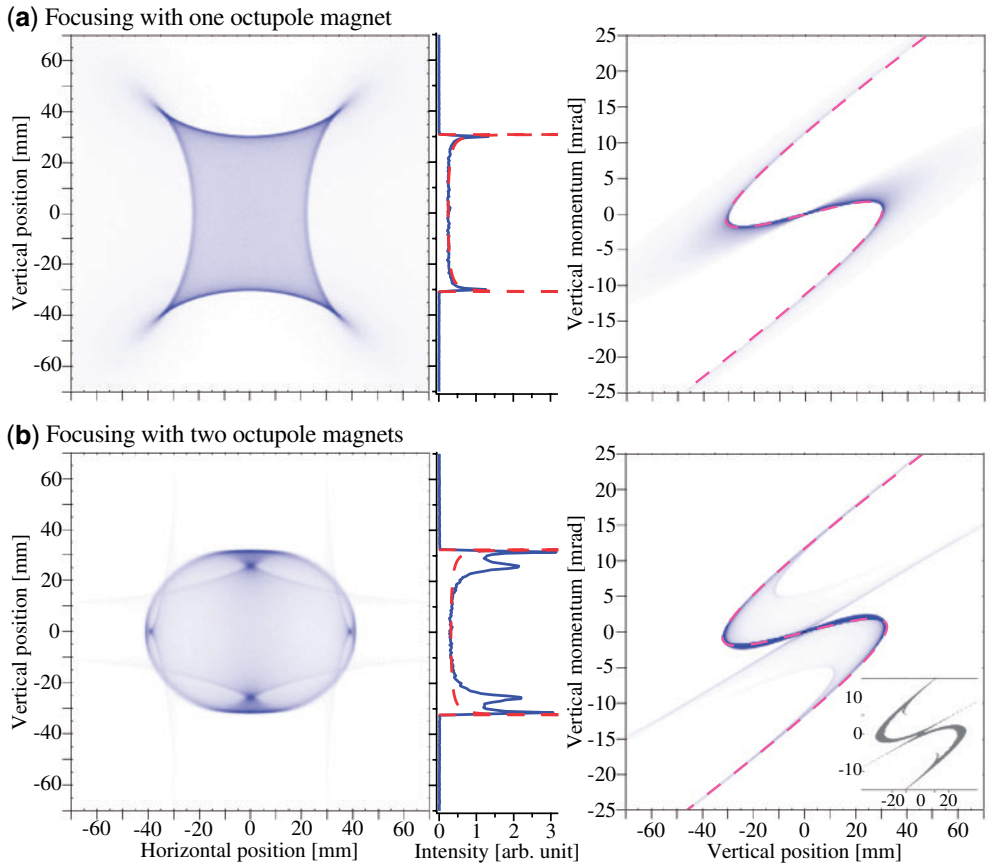


**Fig. 2.** Tracking simulation result of the intensity distributions for the 10-MeV proton beam focused using (a) one or (b) two octupole magnets. The linear beam optics is the same as in Fig. 1. The field gradients ($K_{OCT1}$, $K_{OCT2}$) of the two octupole magnets are (a) (0 $m^{-4}$, 3100 $m^{-4}$) and (b) (-10 500 $m^{-4}$, 3100 $m^{-4}$). The left panels are the relative intensity distributions of the beam cross-section. The middle panels are the 1D relative intensity distributions along the vertical axis. The red dashed lines are the results numerically obtained from Eq. (4). The right panels are the phase-space distributions in the vertical direction. The pink dashed curves are the results numerically obtained from Eqs. (2) and (3). The region of the 80% beam emittance is shown as a gray area in the inset of (b).

When the two octupole magnets are excited properly, the tips are focused inward and thus an elliptical cross-section is formed, as shown in Fig. 2(b). The steep high-intensity peak that surrounds the central low-intensity part of the beam is generated in the periphery of the beam. The peripheral edge of the beam is distinct as the beam intensity is very low at the outside of the edge. The peak height is not even along the edge but is maximized near the horizontal and vertical axes. The contrast, defined here as the ratio of the peak intensity to the intensity around the beam center, is 11 at the maximum. The peak width of the beam is 1 mm for the full width at half maximum (FWHM). The eight "streaks" have grown from the four peaks slightly inside the edge on the axes due to a strong nonlinear kick of ions with large betatron amplitude at the octupole magnets. The transverse phase-space shape of the beam, which is originally an elongated ellipse when no nonlinear force is applied, has been bent into an "S"-shape due to the third-order nonlinear force, as shown in the right panels of Fig. 2. It is found that the 80% emittance, defined as the phase-space area occupied by 80% of the constituent particles, has been increased to $90\pi$ mm·mrad in the case of Fig. 2(b)

because of this deformation of the phase-space distribution. It is, therefore, noteworthy that a sharp peak is generated at the radial edge although the effective emittance is rather increased.

These beam characteristics obtained from the tracking simulation are compared with the theoretical results discussed above. The on-axis spatial distribution calculated using Eq. (4) has been superimposed as a red dashed line in the middle panels of Fig. 2, which properly reproduces the edge position of the simulation result (except for the inner peaks due to the coupling effect in Fig. 2(b)). The phase-space shape calculated from Eqs. (2) and (3) has also been superimposed as a pink dashed curve in the right panels of Fig. 2; this agrees well with the S-shape of the simulation result.

As already shown in Fig. 2, the hollow beam has a radial edge of the steep peak. The edge position corresponds to the point where the beam is sharply bent in the on-target $(x_t - p_t)$ phase space. Namely, the condition $dx_t/dp_t = 0$ is fulfilled at the edge. Since this condition can be rewritten as $dx_t/dp_t = (dx_t/dx_1)\,(dp_t/dx_1)^{-1} = 0$, particles at the edge position satisfy the condition $dx_t/dx_1 = 0$. When this condition holds true, the right-hand side of Eq. (4) diverges infinitely, and thus the intensity distribution of the beam naturally has a high-intensity peak at the edge. The edge positions obtained using Eq. (2) are 4.0 cm and 3.2 cm in the horizontal and vertical directions, respectively, in the case of Fig. 2(b), which agrees with the tracking simulation result.

### *3.3. Dependence of beam emittance*

Equations (2) and (3) indicate that the phase-space shape and thus edge position of the multipole-focused beam do not depend on beam emittance because the emittance $\varepsilon$ is not explicitly included there. On the other hand, the on-target spatial distribution should depend on $\varepsilon$ through the initial distribution of the beam, as shown in Eq. (4). Therefore, the dependence of beam emittance on the hollow-beam profile is investigated. The results are shown in Fig. 3. The primary S-shape of the phase space and the edge position are almost the same even though there is a sixfold difference in the rms emittance. However, the particle distribution around the S-shaped curve actually depends on the emittance. When the initial emittance of the beam is larger, the background particles are increased due to the stronger nonlinear force and thus the beam loss is induced. In addition to the S-shape, a lower-intensity linear structure has been enhanced in the phase space, which corresponds to the above-mentioned streaks in the real-space profile.

## 4. Experiment

### *4.1. Conditions*

The beam experiment was conducted at the TIARA cyclotron facility to demonstrate various hollow-beam shapings using multipole magnets experimentally. The ion species chosen for the experiment was a 10-MeV proton (magnetic rigidity of 0.46 Tm) as the reproducibility of its beam characteristics, such as the spatial profile and emittance, was relatively high among the various ion species that could be accelerated by the cyclotron. The gradients of quadrupole magnets in the beam line were set so that the linear beam optics, the same as in Fig. 1, could be realized. The beam size at the target was relatively large (5–10 cm) to conduct the tuning and measurement of the cross-sectional profile (using sensitive phosphor screens and radiochromic films placed on the target) more readily. The space-charge effect was negligible because the beam current was reduced to the order of 1 nA to obtain moderate light intensity from the screens.

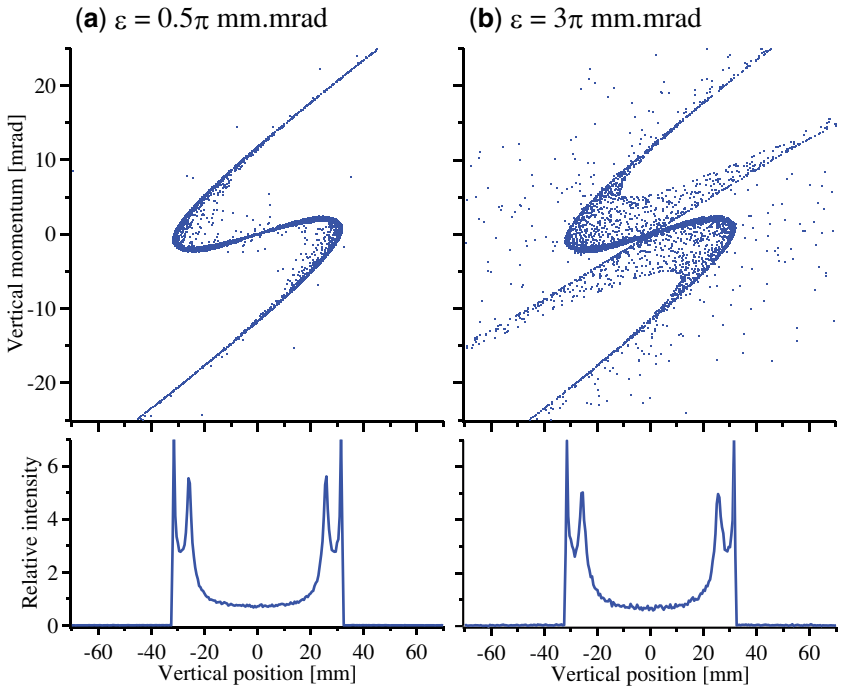


**Fig. 3.** Emittance dependence on the hollow-beam profile. The initial rms emittance of the beam has been set at (a) $0.5\pi$ mm·mrad and (b) $3\pi$ mm·mrad in both transverse directions. The upper panels are the phase-space distributions in the vertical direction. Here, real particles tracked in the simulation are plotted for better visibility. The lower panels are the 1D spatial distributions along the vertical axis. The simulation parameters including the octupole-field gradients are the same as those in Fig. 2(b) except for the rms emittance.

### *4.2. Results*

Figure 4 shows several on-target real-space intensity distributions of the octupole-focused beam. In Figs. 4(a) and 4(b), the cross-sectional profiles, very similar to the profiles in Figs. 2(a) and 2(b), respectively, are formed since the same octupole strengths as those in Fig. 2 are applied to the beam. The eight streaks of the elliptical hollow beam in Fig. 4(b) can be removed by cutting off the original beam's tail using horizontal and vertical beam-defining slits located 2.2 m before the first octupole magnet. Following this beam collimation, the resultant cross-sectional shape of the hollow beam is nearly circular (or ring-shaped), as shown in Fig. 4(c).

Furthermore, the cross-sectional shape of the hollow beam can be changed in the same linear beam optics by simply adjusting the strengths of the two octupole magnets. Figures 4(d) and 4(e) show a rounded rectangle and rhombus, respectively, whose nonlinear-force-induced streaks have been removed in the abovementioned way. In addition to the experiment, we have verified, through systematic simulations, that the cross-sectional shape of the hollow beam changes with the strength of the applied octupole forces. These observation results suggest that the cross-sectional shape of the hollow beam depends on the degree of nonlinear betatron coupling, unlike the case of the rectangular uniform-beam formation in the optics where the betatron coupling is sufficiently suppressed.

The contrast and width of the edge peak are evaluated for the characterization of the hollow beam. The maximum contrast is 14 in Figs. 4(b) and 4(c) and over 20 in Figs. 4(d) and 4(e). The width of the peripheral peak is 1–2 mm in FWHM. Here, while the beam size is much larger, the observed contrast and peak width of the edge are, respectively, higher and smaller than those of the hollow beams generated using the plasma lens [6,7].

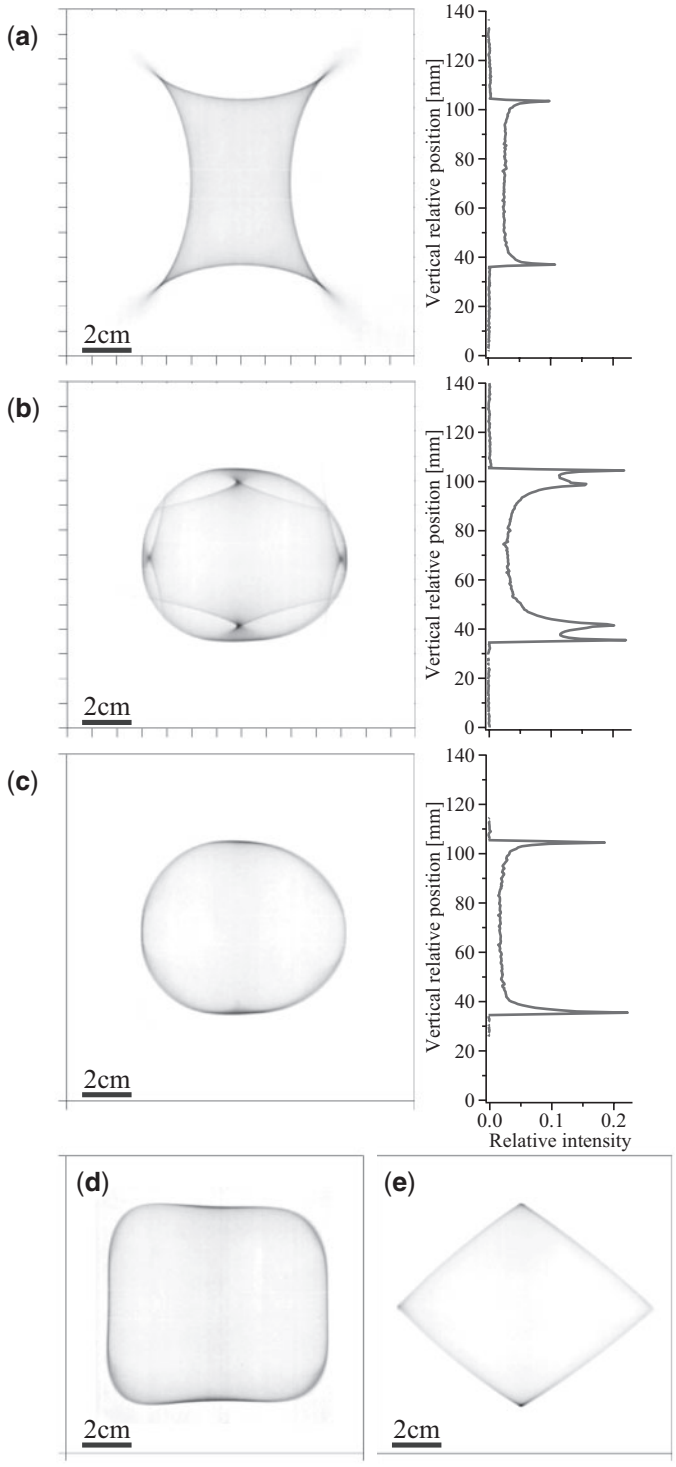


**Fig. 4.** Spatial intensity distributions of the 10-MeV proton beam focused with (a) one or (b)–(e) two octupole magnets. The field gradients ($K_{OCT1}$, $K_{OCT2}$) of the excited two octupole magnets correspond to (a) (0 $m^{-4}$, 3100 $m^{-4}$), (b) and (c) (-10 500 $m^{-4}$, 3100 $m^{-4}$), (d) (-6700 $m^{-4}$, 2400 $m^{-4}$), and (e) (-11 300 $m^{-4}$, 2300 $m^{-4}$). The right panels in (a)–(c) are the 1D distributions along the vertical central axis of the beam. These intensity distributions were obtained using radiochromic films [18].

## 5. Discussion

In the experiment, it is sometimes difficult to survey various parameter dependences of hollow beams comprehensively. In this section, results of systematic tracking simulations are, therefore, described to discuss various characteristics of hollow beams.

### *5.1. Characteristics of hollow beams*

As demonstrated in the experiment above, the shape of the hollow beam depends on the applied octupole force. Therefore, the characteristics of the hollow beams also change with the octupole force and beam optics. As an example, the maximum contrast of the hollow beam and the ratio of particle concentration at the edge peak are surveyed as a function of the octupole strength. As shown in Fig. 5, a contrast higher than 20 can be reached and more than 50% of the constituent particles in the beam are concentrated in the radial peak region for the present beam optics.

Moreover, it has been confirmed that the cross-sectional shape of the hollow beam can be transformed into nearly a circle, rounded square, or 45-degree-rotated square by changing the gradient of quadrupole magnets near the target, i.e., by adjusting the linear beam optics.

### *5.2. Effect of momentum spread*

Next, the effect of the longitudinal momentum spread on the on-target distribution is investigated. The momentum dispersion in the horizontal direction is not very large (about 6.5 m and 7.5 m at the octupole magnets and at the target, respectively) in the present beam optics. When the rms momentum spread of the beam is on the order of $10^{-4}$, which is close to typical values for beams extracted from the TIARA cyclotron [19], the cross-sectional shape of the hollow beam is almost the same although the peak intensity of the hollow beam is slightly decreased.

### *5.3. Effect of sextupole focusing*

Finally, it is informative to discuss the effect of nonlinear focusing of a different order on the beam profile. Figure 6 shows the on-target beam profile when the beam is focused by two sextupole magnets instead of two octupole ones. Obtaining a high-contrast hollow beam is possible. The cross-sectional shape is similar to a triangle owing to the symmetry of the sextupole nonlinear field. The on-target beam is displaced horizontally due to the deflecting effect of sextupole magnets [20].

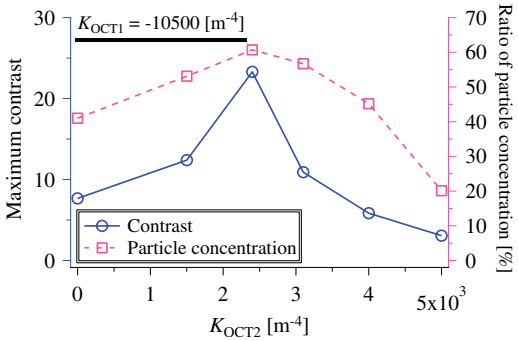


**Fig. 5.** Dependence of the maximum contrast (left axis) and ratio of particle concentration at the edge peak (right axis) on the octupole field gradient $K_{OCT2}$. The linear beam optics is the same as that in Fig. 1 and $K_{OCT1}$ is fixed at -10 500 m$^{-4}$.

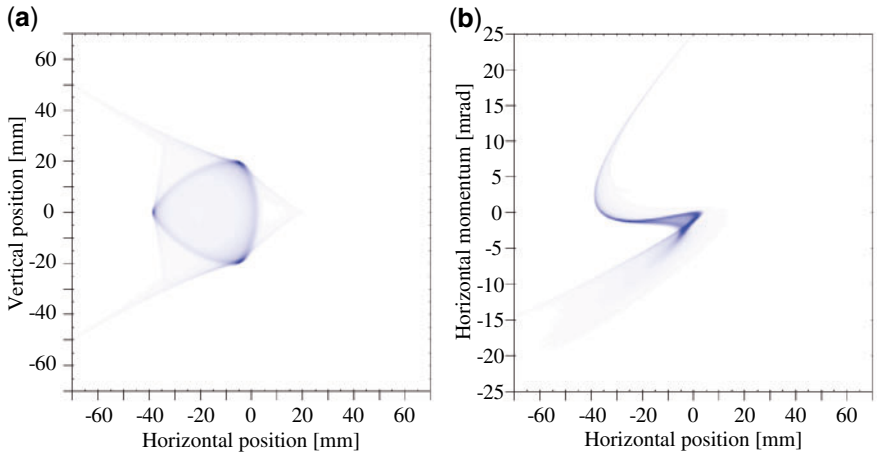


**Fig. 6.** (a) Real-space and (b) phase-space intensity distributions of the beam focused using two sextupole magnets. The sextupole field gradients are 150 $m^{-3}$ and -37 $m^{-3}$.

By comparing Fig. 6 with Figs. 2 and 4, it is obvious that the symmetry of the cross-sectional profile depends on the order of the multipole force. The present result suggests that different cross-sectional shapes of a beam can be realized using higher-order multipole magnet, e.g., decapole and dodecapole magnets.

## 6. Conclusion

The formations of various hollow ion beams using octupole and sextupole magnets in a beam transport line have been theoretically, numerically, and experimentally investigated. Analytical expressions have been derived to predict the phase-space shape, edge position, and real-space distribution of the beam focused by octupole magnets, which are helpful in the design of the beam line and target. The hollow beam can be primarily characterized by the Twiss parameters, the betatron phase advance, and the strength of multipole magnets (although the 2D theoretical analysis of the shape and distribution in the beam cross-section is unsolved owing to the complexity of nonlinear betatron coupling). The hollow beams have a distinct edge with a high contrast (over 20) and a narrow width (1 mm in FWHM). The cross-sectional shape of the beam can be easily changed through the order and strength of the applied multipole magnets (together with the linear beam optics). The proposed method, based on existing accelerator technologies, is useful not only for forming a hollow beam but also for non-destructively generating a specific clear-cut beam that cannot be realized in linear beam optics.

### Acknowledgements

This work was supported in part by Japan Society for the Promotion of Science (JSPS) KAKENHI (Grant Number JP18K11934).

## References

[1] M. Heiß, B. E. Fischer, B. Jakob, C. Fournier, G. Becker, and G. Taucher-Scholz, Radiat. Res. **165**, 231 (2006).
[2] M. Oikawa, T. Satoh, T. Sakai, N. Miyawaki, H. Kashiwagi, S. Kurashima, S. Okumura, M. Fukuda, W. Yokota, and T. Kamiya, Nucl. Instrum. Meth. Phys. Res. B **260**, 85 (2007).
[3] Th. Haberer, W. Becher, D. Schardt, and G. Kraft, Nucl. Instrum. Meth. Phys. Res. A **330**, 296 (1993).
[4] A. M. Koehler, R. J. Schneider, and J. M. Sisterson, Med. Phys. **4**, 297 (1977).

[5] T. R. Renner and W. T. Chu, Med. Phys. **14**, 825 (1987).
[6] U. Neuner et al., Phys. Rev. Lett. **85**, 4518 (2000).
[7] A. Drozdowskiy, N. Alexeev, S. Drozdowskiy, A. Golubev, A. Kuznetsov, Yu. Novozhilov, S. Savin, B. Sharkov, and V. Yanenko, Proc. 1st Int. Particle Accelerator Conf., p. 1062 (2010).
[8] G. Stancari, A. Valishev, G. Annala, G. Kuznetsov, V. Shiltsev, D. A. Still, and L. G. Vorobiev, Phys. Rev. Lett. **107**, 084802 (2011).
[9] J. W. Stetson, G. Machicoane, F. Marti, P. Miller, M. Steiner, P. Zavodzsky, and N. Y. Kazarinov, Proc. 17th Int. Conf. Cyclotrons and their Applications, p. 483 (2004).
[10] N. Yu. Kazarinov, Rev. Sci. Instrum. **75**, 1665 (2004).
[11] Y. Batygin, A. Goto, and Y. Yano, Proc. 1995 Particle Accelerator Conf., p. 1001 (1995).
[12] N. Tsoupas et al., Phys. Rev. ST Accel. Beams **10**, 024701 (2007).
[13] A. Bogdanov, V. Anferov, M. Ball, D. V. Baxter, V. P. Derenchuk, A. V. Klyachko, T. Rinckel, and K. Solberg, Proc. 2007 Particle Accelerator Conf., p. 1748 (2007).
[14] Y. Yuri, T. Ishizaka, T. Yuyama, I. Ishibori, S. Okumura, and K. Yoshida, Nucl. Instrum. Meth. Phys. Res. A **642**, 10 (2011).
[15] S. Meigo, M. Ooi, K. Ikezaki, A. Akutsu, and H. Fujimori, Proc. 5th Int. Particle Accelerator Conf., p. 896 (2014).
[16] Y. Yuri, N. Miyawaki, T. Kamiya, W. Yokota, K. Arakawa, and M. Fukuda, Phys. Rev. ST Accel. Beams **10**, 104001 (2007).
[17] K. Arakawa et al., Proc.13th Int. Conf. Cyclotrons and their Applications, p. 119 (1992).
[18] Y. Yuri, T. Ishizaka, T. Agematsu, T. Yuyama, H. Seito, and S. Okumura, Nucl. Instrum. Meth. Phys. Res. B **406**, 221 (2017).
[19] S. Okumura, N. Miyawaki, S. Kurashima, K. Yoshida, M. Fukuda, I. Ishibori, T. Agematsu, T. Nara, Y. Nakamura, and K. Arakawa, Proc. 17th Int. Conf. Cyclotrons and their Applications, p. 410 (2004).
[20] Y. Yuri, T. Yuyama, T. Ishizaka, I. Ishibori, and S. Okumura, J. Phys. Soc. Jpn. **81**, 064501 (2012).